An Advanced MoS_2/Carbon Anode for High-Performance Sodium-Ion Batteries

*Jingjing Wang, Chao Luo, Tao Gao, Alex Langrock, Alice C. Mignerey, and Chunsheng Wang**

Molybdenum disulfide (MoS_2) is a promising anode for high performance sodium-ion batteries due to high specific capacity, abundance, and low cost. However, poor cycling stability, low rate capability and unclear electrochemical reaction mechanism are the main challenges for MoS_2 anode in Na-ion batteries. In this study, molybdenum disulfide/carbon (MoS_2/C) nanospheres are fabricated and used for Na-ion battery anodes. MoS_2/C nanospheres deliver a reversible capacity of 520 mAh g^{-1} at 0.1 C and maintain at 400 mAh g^{-1} for 300 cycles at a high current density of 1 C, demonstrating the best cycling performance of MoS_2 for Na-ion batteries to date. The high capacity is attributed to the short ion and electron diffusion pathway, which enables fast charge transfer and low concentration polarization. The stable cycling performance and high coulombic efficiency (~100%) of MoS_2/C nanospheres are ascribed to (1) highly reversible conversion reaction of MoS_2 during sodiation/desodiation as evidenced by ex-situ X-ray diffraction (XRD) and (2) the formation of a stable solid electrolyte interface (SEI) layer in fluoroethylene carbonate (FEC) based electrolyte as demonstrated by fourier transform infrared spectroscopy (FTIR) measurements.

1. Introduction

Lithium-ion batteries, the main energy supply for portable electronics, are considered as the prime candidate to power next generation of electric vehicles (EVs) and hybrid electric vehicles (HEVs).[1–3] However, the concerns on the availability and distribution of lithium resource in the earth's crust render the necessity to develop new battery chemistries. Among them, sodium-ion batteries have attracted much attention due to low cost, large resource availability, and similar insertion chemistry with lithium ions.[4–6] Inspired by Li-ion battery chemistry, a large number of cathode materials such as transitional metal oxides were investigated in Na-ion batteries.[7,8] However, there are not as many attempts on improving electrochemical performance of anode materials as that for cathode materials. Up to now, proposed anode materials include carbonaceous materials,[9] Na-alloys (Sn, Sb)[10,11] and binary compounds (metal oxides, metal sulfides).[12–14] Due to the similar chemistry to Li-ion batteries, carbonaceous anode materials are widely used in Na-ion batteries.[15] Recent reports on carbon nanosheet derived from peat moss[16] and hollow carbon nanowires[17] demonstrate a reversible sodium-ion intercalation/deintercalation with specific capacities in the range of 200–300 mAh g^{-1}. Some metals (Sn, Sb) can alloy with Na exhibiting high capacities of 400–600 mAh g^{-1}.[10,11] However, it is very difficult to maintain the high capacity during charge/discharge cycles due to large volume change. To this regard, anode materials with high capacity and superior cycling stability are urgently needed for Na-ion batteries.

J. Wang, Prof. A. C. Mignerey
Department of Chemistry and Biochemistry
University of Maryland
College Park, Maryland 20742, USA
C. Luo, T. Gao, A. Langrock, Prof. C. Wang
Department of Chemical
and Biomolecular Engineering
University of Maryland
College Park, Maryland 20742, USA
E-mail: cswang@umd.edu

DOI: 10.1002/smll.201401521

Recently, there is growing research interest on layered MoS_2 as anode material for Li-ion[18,19] and Na-ion batteries[20] because the unique layered structure is favorable for initial ion intercalation/de-intercalation, and the followed conversion chemistry enables high theoretical capacity. Molybdenum disulfide (MoS_2) is one of two-dimensional transition metal dichalcogenides (TMDs).[21,22] MoS_2 has a lamellar structure with each layer stacking via Van der Waals interactions. In a single-layered MoS_2, there are numerous S-Mo-S units where molybdenum atoms are sandwiched in the center by sulfur atoms with strong covalent bonding. Due to structural similarity to graphite but larger interlayer space, MoS_2 has been explored as anode for high power Li-ion batteries.[23–25] The lithiation process of MoS_2 was depicted as an initial insertion process followed by a conversion reaction, leading to the formation of metallic Mo and Li_2S.[26–29] However, the delithiation mechanism is still on the debate. It is unclear whether the delithiation process is dominated by the oxidation of Mo metal to MoS_2 or the oxidation of Li_2S to S.[30,31]

Due to the chemical similarity between lithium ion and sodium ion, MoS_2 can also be used in Na-ion batteries. David et al. reported MoS_2/graphene paper for Na-ion batteries and revealed the conversion reaction mechanism for MoS_2 and Na ions during sodiation.[20] However, the desodiation mechanism was not elucidated clealy. According to the conversion reaction between one MoS_2 molecule and four sodium ions, the theoretical capacity of MoS_2 is 670 mAh g^{-1}.[32] However, the MoS_2/graphene paper still suffers from low capacity (230 mAh g^{-1}) and poor cycle life (only 20 cycles). Thus, advanced nanostructure fabrication and fundamental understanding of the sodiation/desodiation mechanism are critical to circumvent the main challenges and obtain a stable cycling performance of MoS_2 anode.

In this study, MoS_2/C nanospheres with three-dimensional flower-like architecture were fabricated for Na-ion battery anode. We demonstrated that MoS_2/C nanospheres react with Na-ion through a fully successive intercalation and conversion reaction. MoS_2/C nanospheres exhibit a specific capacity of 520 mAh g^{-1} at 0.1 C and maintain 400 mAh g^{-1} at 1 C for 300 cycles. To our best knowledge, MoS_2/C nanospheres demonstrate one of the best electrochemical performances as anode materials in Na-ion batteries. High cycling stability of MoS_2/C nanospheres is attributed to the formation of a stable solid electrolyte interface (SEI) layer on MoS_2/C nanospheres in fluoroethylene carbonate (FEC)-based electrolyte, and fully reversible conversion reaction of MoS_2 during sodiation/desodiation. Our work on MoS_2/C nanospheres for Na-ion battery anode sheds light on electrode material design, cycling stability improvement and discharge mechanism investigation for future research.

2. Results and Discussion

2.1. Material Characterization

The crystal structures of as-prepared MoS_2 nanosheets and MoS_2/C nanospheres were characterized using X-ray diffraction (XRD) as shown in **Figure 1**a. The diffraction profiles demonstrate the phase purity of MoS_2 with crystallized hexagonal structure (JCPDS 65–0160). MoS_2/C nanospheres show conspicuous peaks at 33° and 59°, which are indexed to (100) and (110) planes of crystalline MoS_2 respectively.[33] The shift of (002) peak from 14.2° to 16.5° is triggered by the intercalation of carbon sheets (amorphous carbon) between MoS_2 sheets and the peak at 16.5° is induced by the interlayer distance between carbon layer and MoS_2 layer.[33–35] Raman spectra of MoS_2 nanosheets and MoS_2/C nanospheres were shown in Figure 1b. The hexagonal layered structure of MoS_2 are indicated by two peaks located at 383 cm^{-1} and 408 cm^{-1}, which are typical first-order Raman active modes E^1_{2g} and A_{1g} due to in-plane vibrational modes within the sulfur-molybdenum-sulfur layer.[36] The Raman spectrum of MoS_2/C nanospheres exhibits two broad bands at 1360 cm^{-1} (D-band) and 1598 cm^{-1} (G-band), besides typical peaks from hexagonal structured MoS_2. The G-band and D-band reveal the presence of in-plane vibration of sp^2-bonded carbon atoms and vibrational modes from sp^3-bonded carbon atoms in amorphous carbon.[37] To determine the weight ratio of MoS_2 to carbon in the sample, thermogravimetric

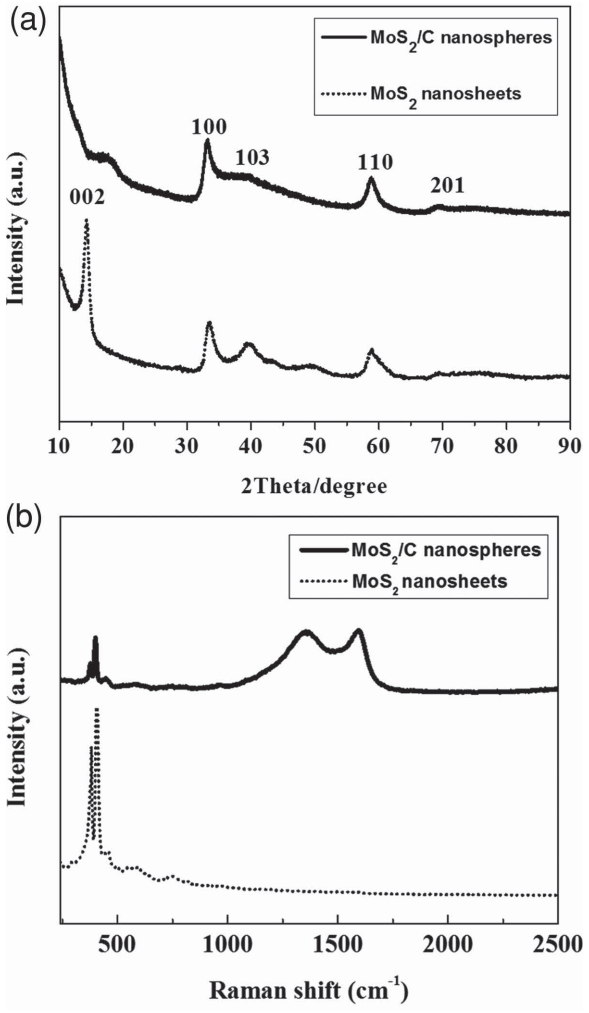

Figure 1. (a) XRD characterization of as-prepared MoS_2 and MoS_2/C nanospheres; (b) Raman spectra of as-prepared MoS_2 and MoS_2/C nanospheres.

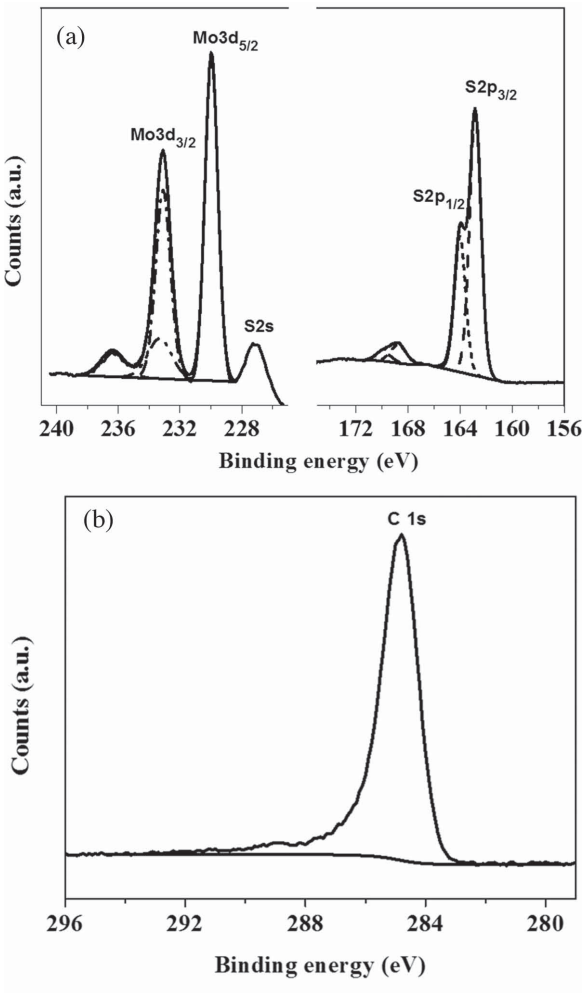

Figure 2. (a) XPS spectra of MoS_2/C composite showing Mo 3d, S 2s; (b) XPS spectra showing C 1s.

analysis (TGA) was carried out from 25 °C to 800 °C in air (Figure S1). The residue of MoS_2/C composite after TGA is MoO_3, as confirmed by X-ray diffraction pattern shown in Figure S2 (MoO_3, JCPDS 005–0508). A major weight loss is observed in the range from 300 °C to 400 °C, which is due to the weight loss induced by oxidation of C into CO_2 and MoS_2 into MoO_3 (Figure S2) with the formation of SO_2 gas.[19,38] TGA result shows that the as-prepared MoS_2/C nanospheres contain 66.7% of MoS_2 and 33.3% of amorphous carbon. **Figure 2** shows X-ray photoelectron spectroscopy (XPS) spectra of MoS_2/C composite with C1s reference peak at 284.8 eV. The presence of MoS_2 and carbon components are demonstrated with characteristic Mo and S with an elemental ratio of ~1:2 and prominent peak of C1s at 284.8 eV. From Figure 2, the Mo3d spectra contain Mo^{6+} $3d_{3/2}$ peak at 236 eV, Mo^{4+} $3d_{3/2}$ peak at 233 eV, $Mo^{4+}3d_{5/2}$ peak at 229 eV and the S 2s peak is detected at 227 eV. The Mo^{6+} $3d_{3/2}$ peak presents with a small portion (18%) as compared with Mo^{4+} 3d, which is possibly due to the oxidation of Mo^{4+} in the atmosphere or the small residue of the reactant Na_2MoO_4. S 2p spin orbit split peaks constrained with a spin orbit splitting of 1.18 eV and an area ratio of 0.5 (S $2p_{1/2}$:S $2p_{3/2}$ = 0.5) as shown in the range of 160–168 eV. The shoulder peak at 169 eV

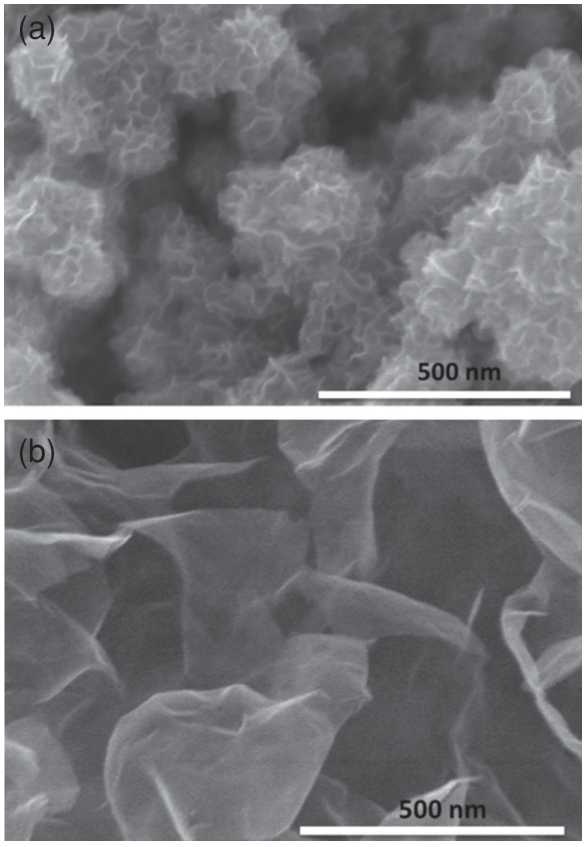

Figure 3. SEM images of (a) MoS_2/C nanospheres; (b) MoS_2 nanosheets.

corresponds to the oxidized sulfur. A sharp peak of C1s is detected at 284.8 eV with a small portion of graphitic carbon in the region of 286–289 eV. The asymmetric peak reveals that carbon exists as a mixture of sp^2 and sp^3 bonding.

The morphology of as-prepared MoS_2/C and MoS_2 is revealed by SEM, TEM images and energy dispersive X-ray spectroscopy (EDS) mapping. As indicated by **Figure 3**, the as-prepared MoS_2 forms two-dimensional nanosheets, while MoS_2/C displays flower-like three-dimensional nanosphere architecture after in situ carbon coating. The introduction of carbon remarkably reduces the size and morphorlogy of MoS_2 nanosheets as evidenced by SEM images. The layered structure of MoS_2/C nanospheres is demonstrated by high-resolution transmission electron microscopy (HRTEM) image (Figure S4). The distinct ring pattern of selected-area electron diffraction (SAED) in the insets of **Figure 4**a and b reveal the crystalline nature of MoS_2 nanosheets and MoS_2/C nanospheres, which is consistent with XRD results in Figure 1a. The existence of amorphous carbon, Mo and S is demonstrated by elemental mapping image of MoS_2/C nanospheres as shown by Figure 4c–f. The EDS mapping confirms that MoS_2 is uniformly distributed in amorphous carbon matrix.

2.2. Electrochemical Performance

The electrochemical properties of MoS_2 nanosheets and MoS_2/C nanospheres are evaluated using coin cells with sodium metal as a counter electrode. **Figure 5**a and b show

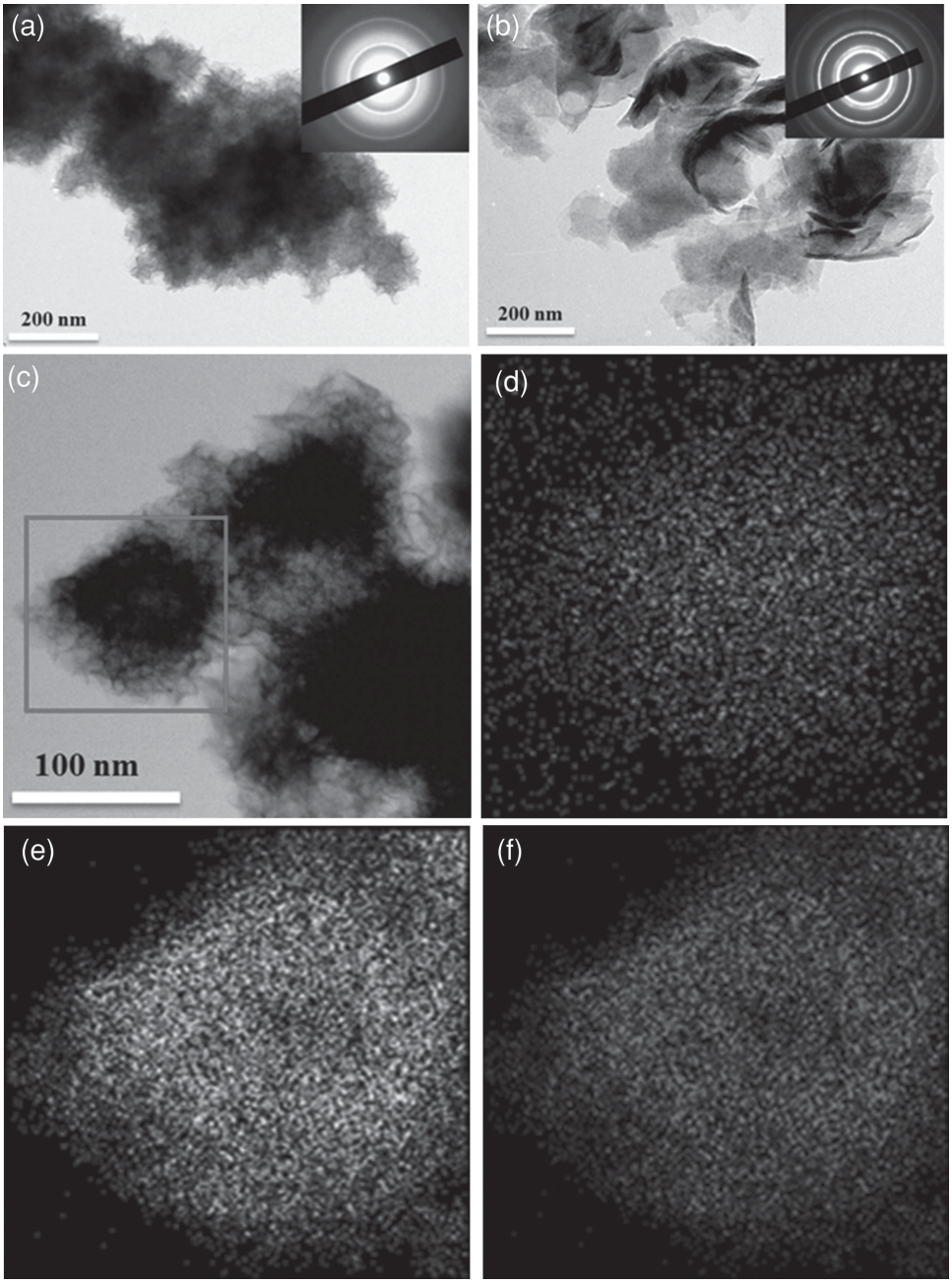

Figure 4. (a) TEM image of MoS_2/C nanospheres (indexed with SAED); (b) TEM image of MoS_2 nanosheets (indexed with SAED); (c) elemental mapping images of MoS_2/C nanospheres; (d) elemental mapping image of C; (e) elemental mapping image of S; (f) elemental mapping image of Mo.

the cyclic voltammograms (CV) of MoS_2 (nanosheets) electrode and MoS_2/C (nanospheres) electrode in initial five cycles respectively. The CV curves of MoS_2 show three reductive peaks at 1.2, 0.7 and 0.005 V and three corresponding oxidation peaks/shoulder at 0.6, 1.7 and 2.2 V in the first cycle. (Figure 5a). In the second sodiation, the reductive peak at 1.2 V shifts to higher potential of 1.4 V, and the intensity of peaks at 0.7 V and 0.005 V are reduced; while the oxidation peaks are slightly increased. The CV peaks are stable during the subsequent four cycles, demonstrating a highly reversible and stable sodiation/desodiation process. The sodiation peak in 1.4 V is attributed to intercalation of sodium ions into MoS_2 interlayer.

$$MoS_2 + xNa^+ + xe^- \rightarrow Na_xMoS_2 \quad (1)$$

The peak at 0.7 V is due to the conversion reaction,

$$Na_xMoS_2 + (4-x)Na^+ + (4-x)e^- \rightarrow 2Na_2S + Mo^{[20]} \quad (2)$$

while the small peak at 0.005 V is ascribed to the Na-ion storage in the interface between Na_2S and Mo, which has been reported in most conversion electrodes.[38] The corresponding three desodiation peaks demonstrate reversed three successive reactions. The intensity decrease of peak at 0.7 V in the following cycles suggests that the SEI film is

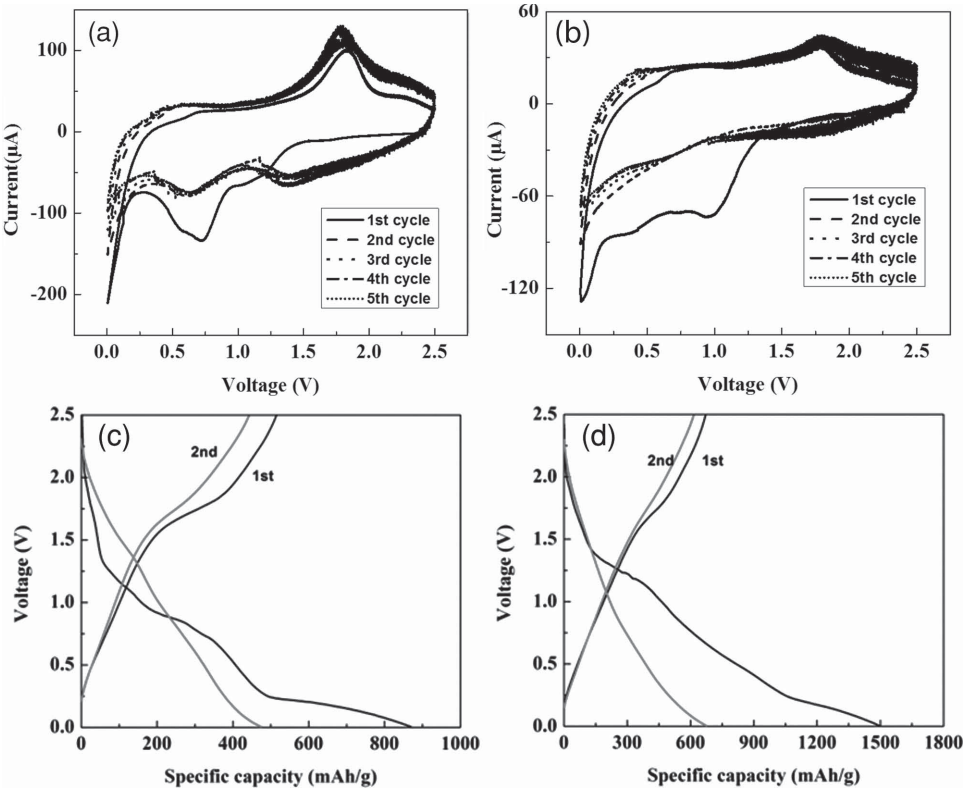

Figure 5. (a) Cyclic voltammograms of MoS_2 electrode and (b) MoS_2/C electrode between 0.005 V–2.5 V with a scan rate of 0.1 mV/s; (c) Charge and discharge profiles of MoS_2 electrode and (d) MoS_2/C electrode vs. Na^+/Na with a cut-off window 0.005–2.5 V.

formed on the electrode surface at this potential. SEI film formation leads to irreversible capacity loss and low coulombic efficiency in the first cycle. The CV scans of MoS_2/C electrode show similar peaks but are less prominent due to interference of Na-ion insertion/extraction to carbon coating layer. In addition, the stable redox peaks in Figure 5a and b illustrate the good cycling stability of MoS_2 electrode and MoS_2/C electrode.

The charge and discharge curves of MoS_2 electrode and MoS_2/C electrode with a cut-off window between 0.005 V and 2.5 V at a current density of 0.1 C are shown in Figure 5c and d. During initial sodiation, three plateaus located at 1.4 V and 0.7 V and 0.2–0.005 V are observed in MoS_2 and MoS_2/C electrodes, which is consistent with the CV scans in Figure 5a and b. As discussed earlier, the first plateau corresponds to the intercalation of sodium ions to MoS_2 interlayer, and the second plateau is ascribed to the conversion reaction, and plateau at 0.2–0.005 V is due to insertion of the Na-ion into the interface between Mo and Na_2S. For MoS_2/C electrode, a sloping curve is observed and no conspicuous potential plateau can be detected in the subsequent sodiation processes, and this phenomenon is consistent with the CV curves of MoS_2/C electrode. However, the sloping plateau at 1.7 V is still visible, revealing the highly reversible oxidation reaction from Mo to MoS_2. Meanwhile, MoS_2/C electrode displays an exceptional high desodiation capacity at 671 mAh g^{-1} in the initial cycle. The capacity of MoS_2/C electrode is very close to the theoretical capacity (670 mAh g^{-1}) of MoS_2, which is calculated based on one MoS_2 molecule reacts with four sodium ions in the conversion reaction (reaction (1) and (2)).

The cycling stability of MoS_2 and MoS_2/C electrodes were investigated at 0.1 C. As indicated by **Figure 6**a, the Coulombic efficiencies of both MoS_2 and MoS_2/C electrodes after 10 cycles are close to 100% (Figure 6a and b), revealing high stability of SEI film formed in FEC-based electrolyte. As a comparison, the cycling performance of MoS_2/C electrode without FEC in the electrolyte show relatively fast capacity fading after 50 fully discharging/charging cycles in Na-ion batteries as demonstrated by figure S5. It has been revealed FEC can stabilize the formation of SEI film on the electrode surface, leading to stable cycling performance.[39] All the specific capacities are calculated based on MoS_2 after subtracting the contribution from carbon, which is about 100 mAh g^{-1} at the same current density (Figure S6). MoS_2/C electrode displays a much higher capacity than that of MoS_2 electrode. According to Figure 6a, MoS_2/C electrode delivers a high capacity (671 mAh g^{-1}) in the first cycle, and retains at 520 mAh g^{-1} for 50 cycles, while MoS_2 electrode delivers a reversible capacity of 360 mAh g^{-1} for 50 cycles. The cycling performance of MoS_2 electrode and MoS_2/C electrode at high current rates is demonstrated in Figure S7 and Figure 6b respectively. During the charge/discharge cycles, both MoS_2 and MoS_2/C electrodes show stable cycling performance in Na-ion batteries. Even at a high current rate of 2 C, the charge capacity of MoS_2/C electrode is 390 mAh g^{-1}, which is an indication of its fast reaction kinetics with sodium ions. After the current density decreases to 0.1 C, the capacity of MoS_2/C electrode recovers to its initial capacity immediately (520 mAh g^{-1}). After rate capacity measurement, the MoS_2/C electrode is further cycled at high current of 1 C to

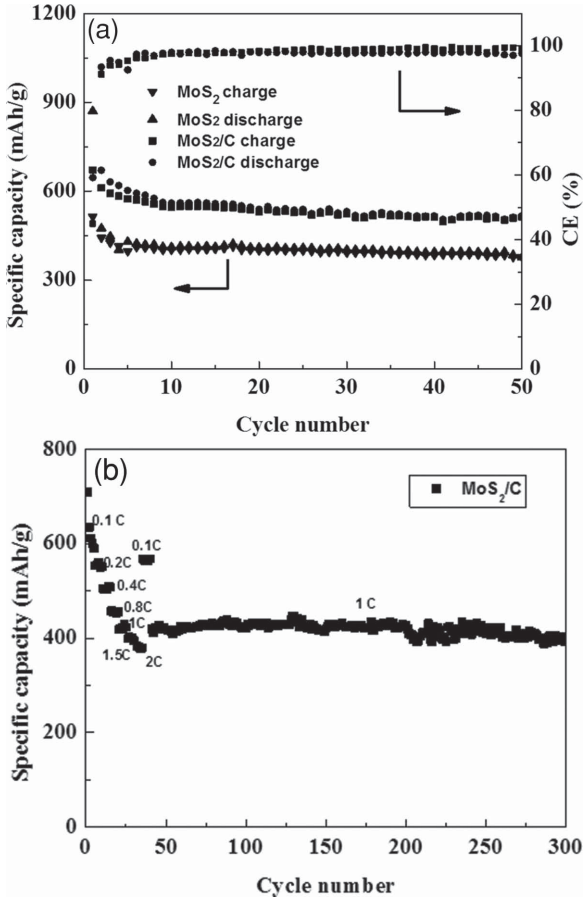

Figure 6. (a) Cycling performance of MoS_2/C electrode in FEC added electrolyte (squares, desodiation cycles; circles, sodiation cycles), and MoS_2 electrode in FEC added electrolyte (down triangles, desodiaiton cycles; up triangles, sodiation cycles) in Na-ion batteries. (b) rate capability of MoS_2/C electrode in Na-ion batteries (1C = 670 mA g^{-1}).

investigate the long-term cycling stability. At 1 C, the MoS_2/C electrode maintains a reversible capacity of 400 mAh g^{-1} for 300 cycles without obvious capacity fading (Figure 6b). Similarly, MoS_2 electrode also shows highly stable cycling capacity although the capacity of MoS_2 is lower than that of MoS_2/C electrode (Figure S7 in supporting information). The higher capacity of MoS_2/C electrode is ascribed to the improved reaction kinetics by carbon coating as further confirmed by electrical impedance spectra (EIS) of both MoS_2 and MoS_2/C electrodes (Figure S8), smaller size and unique flower-like morphology. The role of carbon coating can be understood in three aspects: (1) smaller particle size: As discussed in our manuscript, the introduction of carbon remarkably reduces the particle size as evidenced by SEM images. (2) morphological change: The as-prepared MoS_2 exhibits nanosheet morphology while the carbon coated MoS_2 displays spherical particles as shown by TEM images. It seems that the colloidal carbonaceous material tends to form a 3D sphere-like morphology.[33,40] (3) better electrical conductivity: The EIS measurements shown in Figure S8 demonstrates that the carbon coating significantly enhances the electrical conductivity of the active material-MoS_2. The small size, large surface area and short ion diffusion pathway enables easier access to Na^+, leading to exceptional battery performance.

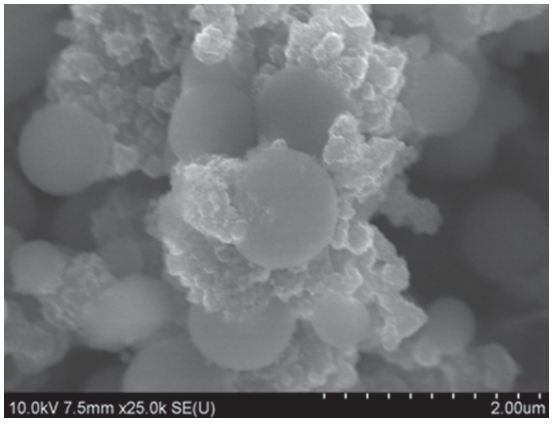

Figure 7. The SEM image of MoS_2/C nanospheres after 50 cycles in Na-ion batteries.

2.3. Mechanism Investigation

The mechanism behind the high coulombic efficiency, high capacity and exceptional cycling stability of MoS_2/C anode is investigated. As stated previously, the high coulombic efficiency of MoS_2/C anode may be attributed to the robustness of the SEI film that can effectively accommodate volume changes. **Figure 7** shows the morphology of MoS_2/C electrode after 50 deep charge/discharge cycles. As evidenced by the SEM image, the SEI coating and volume expansion during sodiation change flower-like MoS_2/C nanospheres into solid spherical nanoparticles and the flower-like morphology of MoS_2/C nanospheres cannot be observed. Meanwhile, the morphology of MoS_2/C electrodes after 50 cycles in FEC electrolyte was characterized using TEM (Figure S9a). Despite the particle size of MoS_2/C nanospheres increased from 200 nm (Figure 4c) to 300 nm due to sodium-ion intercalation/de-intercalation, the regular nanosphere morphology is still maintained in FEC electrolyte. A shell is formed on the surface of flower-like MoS_2/C nanospheres, demonstrating the formation of SEI film on the surface of MoS_2/C nanospheres. The SEI layer on MoS_2/C electrode was further confirmed by FTIR. **Figure 8** shows the FTIR spectra of MoS_2/C nanospheres, fresh MoS_2/C electrode and cycled MoS_2/C electrode. The cycled MoS_2/C electrode was immersed in diethylcarbonate (DEC) for 24 hours to remove $NaPF_6$. As indicated by Figure 8, there are two conspicuous peaks at 1400 cm^{-1} and 1572 cm^{-1} in the spectra of cycled MoS_2/C electrode, representing the stretching vibration of the carbonate groups of FEC and DMC in SEI layer,[41] while peaks at 1400 cm^{-1} and 1572 cm^{-1} are absent in the spectra of MoS_2/C powder and fresh MoS_2/C electrode.

The conversion reaction mechanism (Na_xMoS_2 + (4-x) Na^+ + $4e^- \rightarrow 2Na_2S$ + Mo) in MoS_2/C electrodes, suggested by CV and galvanostatic charge/discharge profiles in Figure 5, was further confirmed by the structural evolution during sodium-ion intercalation and extraction. *Ex-situ* XRD studies were carried out to compare the composition changes of fresh MoS_2/C electrode, fully discharged and charged electrodes as plotted in **Figure 9**. To understand the structural changes at sodiation state, the cell was fully discharged to 5 mV. The cycled cell was first fully discharged to 5 mV,

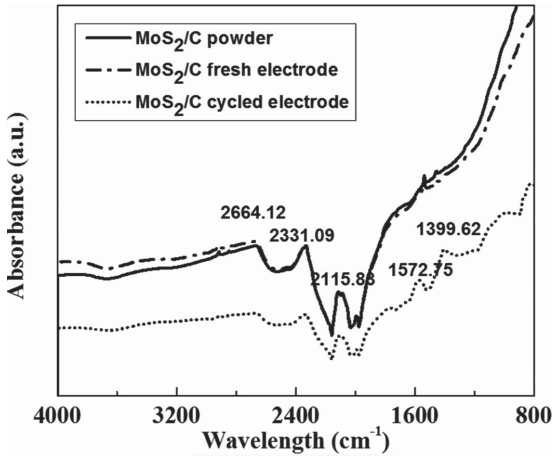

Figure 8. FTIR spectra of MoS_2/C nanosphere powders (black curve), fresh MoS_2/C electrode without cycling (dash curve), and MoS_2/C electrode after charge/discharge cycles in Na-ion batteries (dot curve).

then charged to 2.5 V and maintained at 2.5 V for 24 hours. Before XRD measurements, the electrode was immersed in DEC to remove $NaPF_6$. From Figure 9, the fresh MoS_2/C electrode shows characteristic (100) peak at 33 degree, suggesting the crystalline structure of MoS_2. The peaks at 43, 51 degrees in the XRD pattern are attributed to the copper current collector. The existence of a peak at 27 degree is due to the addition of carbon black in the electrode. After sodiation (discharge), the MoS_2 in MoS_2/C electrode converts to Mo and Na_2S. The existence of Na_2S was revealed by its characteristic peak at 39 degree (JCPDS No. 03–0933) and weak signal from unreacted MoS_2 was shown in fully discharged cell. No crystal Mo peaks can be observed in the discharged MoS_2/C electrode, probably due to the formation

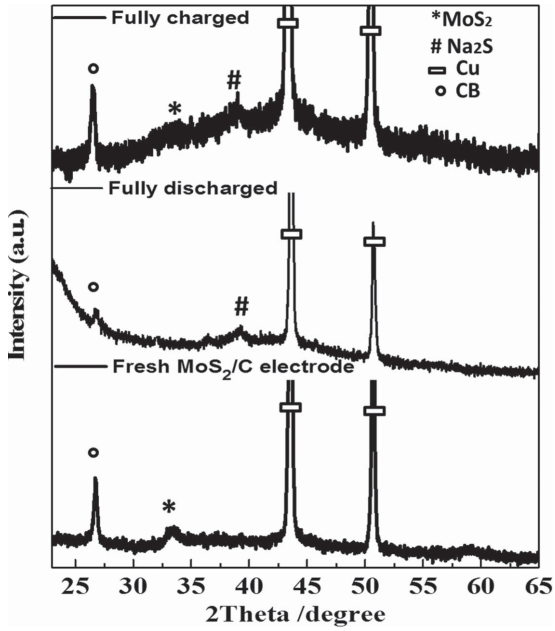

Figure 9. Structural changes of MoS_2/C electrodes before and after discharge/charge cycles (peaks of MoS_2 are labeled as *, # for Na_2S, squares for Cu current collector and circles for carbon black).

of amorphous Mo.[42,43] At desodiation state after one fully discharge/charge cycle, the existence of crystalline MoS_2 was observed as evidenced by the characteristic (100) peak at 33 degree. It is worth noticing that a small peak of Na_2S was also observed in fully charged electrode, which is due to the incomplete reaction of Na_2S during desodiation process. Meanwhile, the crystalline sulfur is not detected, suggesting the complete reaction from Na_2S to MoS_2 rather than S during desodiation.

It was reported that the lithiation/delithiation of MoS_2 experienced irreversible conversion reaction.[42] During the first lithiation, MoS_2 electrochemically dissociates irreversibly into Li_2S and Mo and then are able to reversibly cycle as a sulfur cathode through reversible reaction of Li_2S + Mo/$Li_x \leftrightarrow$ S + Mo + Li_{x+2}. To validate the reversible conversion reaction of MoS_2/C for Na-ion is not due to the special morphology of MoS_2/C nanospheres, the phase structure of fully delithiated MoS_2/C electrode after fully lithiation to 0.01 V was also investigated using *ex-situ* XRD and shown in figure S10. There is no conspicuous peak for MoS_2 after the MoS_2/C electrode was charged to 3.0 V, which is consistent with previous literatures.[42] Therefore, MoS_2 electrochemically reacts with Na ions through reversible conversion reaction, while it reacts with Li ions through oxidation/reduction of Li_2S after first lithiation to form Li_2S/Mo composite.

3. Conclusion

Flower-like MoS_2/C nanospheres were fabricated as Na-ion battery anodes. MoS_2/C nanospheres show high capacity, long cycle life and exceptional rate capability in Na-ion batteries. MoS_2/C nanospheres deliver a reversible capacity of 520 mAh g^{-1} at a current density of 0.1 C. After increasing the current density to 1 C, MoS_2/C nanospheres maintain a specific capacity of 400 mAh g^{-1} for 300 cycles, demonstrating its exceptional cycling ability and fast reaction kinetics. Such an excellent electrochemical performance of MoS_2/C anode in Na-ion batteries is ascribed to the carbon coating, small size and the formation of a stable SEI layer. The superior battery performance of MoS_2/C nanospheres demonstrates that MoS_2 is a promising anode material for Na-ion batteries. Furthermore, the reversibility of the conversion reaction between MoS_2 and sodium ions was demonstrated by *ex-situ* XRD. Our investigation on the electrochemical performance and sodiation/desodiation mechanism of MoS_2/C nanospheres paves the way for the feasibility of high-performance Na-ion batteries.

4. Experimental Section

Synthesis of Nanostructured MoS_2: All chemicals were purchased from Sigma Aldrich and used as received. A mass of 100 mg of $Na_2MoO_4 \bullet 2H_2O$ and 133 mg of NH_2CSNH_2 were dissolved and stirred for 10 min in 20 mL deionized water. The solution was then transferred into a Teflon-lined stainless steel autoclave and annealed at 240 °C for 24 h. After that, the black precipitates were collected by centrifugation, washed with deionized water for three

times and ethanol for once, and dried in a vacuum oven at 80 °C for 12 h.

The reaction mechanism of the synthesis process is shown below:

$$4Na_2MoO_4 + 15CS(NH_2)_2 + 6H_2O \rightarrow 4MoS_2 + Na_2SO_4 + 6NaSCN + 24NH_3(g) + 9CO_2(g)$$

Synthesis of MoS_2/C Nanospheres: All chemicals were purchased from Sigma Aldrich and used as received. 100 mg of $Na_2MoO_4 \bullet 2H_2O$ and 133 mg of NH_2CSNH_2 were dissolved in 20 mL deionized water, and then 334 mg of sucrose was added into the solution. After stirring for 10 minutes, the solution was clear and transferred into a Teflon-lined stainless steel autoclave. The reaction started after heat treatment at 240 °C for 24 h. After that, the black precipitates were collected by centrifugation, washed with deionized water and ethanol, and dried in a vacuum oven at 80 °C for 12 h. The MoS_2/C nanospheres were annealed in a conventional tube furnace at 800 °C for 2 h in a stream of 5% hydrogen in argon flow.

Material Characterization: SEM images were taken by Hitachi SU-70 analytical ultra-high resolution SEM (Japan); TEM images were taken by JEOL (Japan) 2100F field emission TEM; TGA was carried out using a thermogravimetric analyzer (TA Instruments, USA) with a heating rate of 5 °C min-1 in argon; XRD pattern was recorded by Bruker Smart1000 (Bruker AXS Inc., USA) using CuKα radiation; Raman measurements were performed on a Horiba Jobin Yvon Labram Aramis using a 532 nm diode-pumped solid-state laser, attenuated to give ~900 μW power at the sample surface. Fourier transform infrared spectroscopy (FTIR) was recorded by NEXUS 670 FT-IR Instrument.

Electrochemical Measurements: The MoS_2 or MoS_2/Carbon powders were mixed with carbon black and sodium alginate binder to form slurry at the weight ratio of 70:20:10. Coin cells for sodium-ion batteries were assembled with sodium foil as the counter electrode, 1 M $NaPF_6$ in a mixture of fluoroethylene carbonate/dimethyl carbonate (FEC/DMC, 1:1 by volume) as the electrolyte and Celgard 3501 as the separator. Electrochemical performance was tested using Arbin battery test station (BT2000, Arbin Instruments, USA). Both the charge and discharge current density and specific capacity were calculated based on the mass of MoS_2 in the electrode. Cyclic voltammograms were recorded using Solatron 1260/1287 Electrochemical Interface (Solatron Metrology, UK) with a scan rate of 0.1 mV/s between 0.005 and 2.5 V (versus Na/Na^+).

Supporting Information

Supporting Information is available from the Wiley Online Library or from the author.

Acknowledgements

We acknowledge the financial support from the Army Research Office under Contract No.:W911NF1110231. We also acknowledge the support of the Maryland NanoCenter and its NispLab. The authors are grateful for the technique help from Prof. Kang Xu, Dr. Panju Shang, Kaitlyn Crawford and Prof. Lawrence R. Sita.

[1] M. Armand, J. M. Tarascon, *Nature* **2008**, *451*, 652.
[2] K. S. Kang, Y. S. Meng, J. Breger, C. P. Grey, G. Ceder, *Science* **2006**, *311*, 977.
[3] C. Luo, Y. Zhu, Y. Wen, J. Wang, C. Wang, *Adv. Funct. Mater.* **2014**, DOI: 10.1002/adfm.201303909.
[4] C. Luo, Y. Xu, Y. Zhu, Y. Liu, S. Zheng, Y. Liu, A. Langrock, C. Wang, *ACS Nano* **2013**, *9*, 8003.
[5] C. Luo, Y. Zhu, T. Gao, Y. Xu, Y. Liu, J. Wang, C. Wang, *J. Power Sources* **2014**, *250*, 372.
[6] A. Abouimrane, D. Dambournet, K. W. Chapman, P. J. Chupas, W. Weng, K. Amine, *J. Am. Chem. Soc.* **2012**, *134*, 4505.
[7] V. Palomares, M. Casas-Cabanas, E. Castillo-Martınez, M. H. Hanb, T. Rojo, *Energy Environ. Sci.* **2013**, *6*, 2312.
[8] N. Yabuuchi, M. Kajiyama, J. Iwatate, H. Nishikawa, S. Hitomi, R. Okuyama, R. Usui, Y. Yamada, S. Komaba, *Nat mater.* **2012**, *11*, 512.
[9] D. A. Stevens, J. R. Dahn, *J. Electrochem. Soc.* **2000**, *147*, 1271.
[10] Y. Liu, Y. Xu, Y. Zhu, J. Culver, C. Lundgren, K. Xu, C. Wang, *ACS Nano* **2013**, *7*, 3627.
[11] Y. Zhu, X. Han, Y. Xu, Y. Liu, S. Zheng, K. Xu, L. Hu, C. Wang, *ACS Nano* **2013**, *7*, 6378.
[12] H. Xiong, M. D. Slater, M. Balasubramanian, C. S. Johnson, T. Rajh, *J. Phys. Chem. Lett.* **2011**, *2*, 2560.
[13] Q. Sun, Q. Ren, H. Li, Z. Fu, *Electrochem. Commun.* **2011**, *13*, 1462.
[14] L. Wu, X. Hu, J. Qian, F. Pei, F. Wu, R. Mao, X. Ai, H. Yang, Y. Cao, *J. Mater. Chem. A* **2013**, *1*, 7181.
[15] L. Dai, D. W. Chang, J.-B. Baek, W. Lu, *Small* **2012**, *8*, 1130.
[16] J. Ding, H. Wang, Z. Li, A. Kohandehghan, K. Cui, Z. Xu, B. Zahir, X. Tan, E. M. Lotfabad, B. C. Olsen, D. Mitlin, *ACS Nano* **2013**, *7*, 11004.
[17] Y. Cao, L. Xiao, M. L. Sushko, W. Wang, B. Schwenzer, J. Xiao, Z. Nie, L. V. Saraf, Z. Yang, J. Liu, *Nano Lett.* **2012**, *12*, 3783.
[18] Y. Shi, Y. Wang, J. I. Wong, A. Y. S. Tan, C.-L. Hsu, L.-J. Li, Y.-C. Lu, H. Y. Yang*Sci. Rep.* **2013**, *3*, 2169.
[19] Y. Wang, G. Xing, Z. J. Han, Y. Shi, J. I. Wong, Z. X. Huang, K. Ostrikov, H. Y. Yang, *Nanoscale* **2014**, DOI: 10.1039/c4nr01553c.
[20] L. David, R. Bhandavat, G. Singh, *ACS Nano* **2014**, doi: 10.1021/nn406156b.
[21] B. Radisavljevic, A. Radenovic, J. Brivio, V. Giacometti1, A. Kis, *Nat. Nanotechnol.* **2011**, *6*, 147.
[22] M. Chhowalla, H. S. Shin, G. Eda, L.-J. Li, K.-P. Loh, H. Zhang, *Nat. Chem.* **2013**, *5*, 263.
[23] G. Du, Z. Guo, S. Wang, R. Zeng, Z. Chen, H. Liu, *Chem. Commun.* **2010**, *46*, 1106.
[24] K. Chang, W. Chen, *Chem. Commun.* **2011**, *47*, 4252.
[25] Y. Miki, Y. D. Nakazato, H. Ikuta, T. Uchida, M. Wakihara, *J. Power Sources* **1995**, *54*, 508.
[26] L. Ch Yang, S.-N. Wang, J.-J. Mao, J.-W. Deng, Q.-Sh. Gao, Y. Tang, O. G. Schmidt, *Adv. Mater.* **2013**, *25*, 1180.
[27] H. Hwang, H. Kim, J. Cho, *Nano Lett.* **2011**, *11*, 4826.
[28] J.-Zh. Wang, L. Lu, M. Lotya, J. N. Coleman, Sh.-L. Chou, H.-K. Liu, A. I. Minett, J. Chen, *Adv. Energy Mater.* **2013**, *3*, 798.
[29] K. Chang, D. Geng, X. Li, J. Yang, Y. Tang, M. Cai, R. Li, X. Sun, *Adv. Energy Mater.* **2013**, *3*, 839.
[30] X. Fang, X. Guo, Y. Mao, Ch. Hua, L. Shen, Y. Hu, Zh. Wang, F. Wu, L. Chen, *Chem. Asian J.* **2012**, *7*, 1013.
[31] T. Stephenson, Zh. Li, B. Olsen, D. Mitlin, *Energy Environ. Sci.* **2014**, *7*, 209.

[32] X. Cao, Y. Shi, W. Shi, X. Rui, Q. Yan, J. Kong, H. Zhang, *Small* **2013**, *9*, 3433.
[33] K. Chang, W.-X. Chen, L. Ma, H. Li, H. Li, F. Huang, Z. Xu, Q. Zhang, J.-Y. Lee, *J. Mater. Chem.* **2011**, *21*, 6251.
[34] G. Huang, T. Chen, W.-X. Chen, Z. Wang, K. Chang, L. Ma, F. Huang, D. Chen, J. Y. Lee, *Small* **2013**, *9*, 3693.
[35] T. Yang, Y. Chen, B. Qu, L. Mei, D. Lei, H. Zhang, Q. Li, T. Wang, *Electrochimi. Acta* **2014**, *115*, 165.
[36] B. C. Windom, W. G. Sawyer, D. W. Hahn, *Tribol Lett.* **2011**, *42*, 301.
[37] M. Sevilla, A. B. Fuertes, *Carbon* **2009**, *47*, 2281.
[38] Z. Wang, T. Chen, W. Chen, K. Chang, L. Ma, G. Huang, D. Chen, J. Y. Lee, *J. Mater. Chem. A* **2013**, *1*, 2202.
[39] S. M. Oh, S. T. Myung, M. W. Jang, B. Scrosati, J. Hassoun, Y. K. Sun, *Phys. Chem. Chem. Phys.* **2013**, *15*, 3827.
[40] X. M. Sun, Y. D. Li, *J. Colloid Interface Sci.* **2005**, *291*, 7.
[41] H. Du, C. T. Williams, A. D. Ebner, J. A. Ritter, *Chem. Mater.* **2010**, *22*, 3519.
[42] J. Xiao, X. Wang, X. Q. Yang, S. Xun, G. Liu, P. K. Koech, J. Liu, J. P. Lemmon, *Adv. Funct. Mater.* **2011**, *21*, 2840.
[43] W.-H. Ryu, J.-W. Jung, K. Park, S.-J. Kima, I.-D. Kim, *Nanoscale* **2014**, DOI: 10.1039/c4nr02044h.

Received: May 29, 2014
Revised: August 8, 2014
Published online: September 25, 2014